Volume 17, Number 1, 2024. pp. 107-115

Jordan Journal of Physics

ARTICLE

Hartree-Fock Calculations of ^{12}C Nucleus at Equilibrium and Under Static Compression

Iyad Alhagaish

Physics Department, Faculty of Science, The Hashemite University, P.O. Box, 330127, Zarqa 13133, Jordan.

Doi: **https://doi.org/10.47011/17.1.10**

Received on: 18/06/2022; *Accepted on: 29/08/2022*

Abstract: The ground state features of the semi-doubly magic ^{12}C nucleus (i.e. binding energy, nuclear radius, radial density distribution, and single particle energies) are estimated using *ab initio* calculations at equilibrium and under high static compression. Nijmegen and Reid soft-core (RSC) potentials are used as input nucleon-nucleon interactions. Within the framework of the constrained spherical Hartree-Fock approximations, we do the calculations in no-core shell-model space, which consists of six major oscillator shells (i.e. 21 single particle orbitals). The sensitivity of the ground state features of the ^{12}C nucleus to the degree of compression and the sensitivity of the equation of state to the two potentials are investigated. We also discovered that the nuclear binding energy calculated using the Nijmegen potential is higher than that calculated using the RSC potential. When utilizing the Nijmegen potential, the curve reaches zero binding energy faster than when using the RSC potential. Besides, in the case of Nijmegen, the spectrum of single-particle energies increases more quickly than in the case of RSC potential under compression. The space between single-particle energy shells is also visible in the energy spectrum. At high compression, the radial density distribution becomes higher than that in the interior zone when the RSC potential is applied.

Keywords: Nijmegen potential, RSC potential, Ab-initio calculations model, Radial density distribution, Ground state, ^{12}C nucleus.

1. Introduction

The essential and challenging problem in the nuclear structure theory is the solution of the Schrodinger equation for a finite nucleus. The analytic solution is impossible (save in a few basic circumstances), thus one must resort to approximation, either in the numerical solution of the equation or in the Hamiltonian specification, or both [1]. The calculations in light nuclei and heavy nuclei with closed shells were done using the NCSM [2]. The inter-nucleon interaction can be represented by a potential for the purposes of studying nuclear structure. Nijmegen [3], Reid soft-core (RSC) [4], CD-Bonn [5], and Argonne V18 [6] have all been used as potential models in the past. Their strong repulsive core, however, causes convergence problems in nuclear structure calculations; hence, none of them can be employed directly in nuclear structure calculations. The Bruckner G-matrix has conventionally been utilized as a starting point to address this challenge [7]. As of late, the *ab initio* no-core shell NSM model with realistic effective NN interactions has been utilized to light nuclei [8-10]. It has been demonstrated that the NCSM approach can be used to solve the three-nucleon and four-nucleon-bound state problems in a consistent manner. The NCSM is based on a new variant of the widely used nuclei shell model. Shell-model calculations have traditionally been done with closed, inert cores of nucleons and only a few active valence

Corresponding Author: Iyad Alhagaish **Email**: iyadk@hu.edu.jo

nucleons. Microscopic interactions, which were created for few-nucleon systems, could not characterize the interaction of these valence nucleons with the core and other valence nucleons. As a result, these attempts to link the effective shell model interaction to the basic nuclear interaction have not been entirely successful. With the development of the NCSM in 1990, which treats all nucleons in the nucleus as active, the situation was changed [11]. The NCSM allows for the systematic calculation of effective interactions using bare NN and 3N forces. Compared to conventional shell model calculations, this is the NCSM's strength [11].

In this article, we applied a realistic effective interaction based on two different potentials, the Nijmegen and Reid soft-core (RSC), to investigate the ground state features of closed shell semi-doubly magic of ^{12}C nucleus under equilibrium conditions, large static compression, and at zero temperature. Within the framework of the constrained spherical Hartree-Fock (CSHF) approximations, the NCSM space has six primary oscillator shells (i.e. 21 single particle orbitals) throughout our calculations. At zero temperature, we explore the susceptibility of the ^{12}C nucleus ground state features, including binding energy, nuclear radius, radial density distribution, and single particle energies, to the strength of compression.

Hartree-Fock is a well-established method for modeling semi-realistic interactions, even for the heaviest nuclei [12], and it's flexible enough to deal with many-body forces [13, 14]. It is also a starting point for several body methods that are widely employed in heavier systems [12]. The choice to focus on ^{12}C is motivated by its significance in neutrino research, particularly in neutrino liquid-scintillator detectors, where ^{12}C plays a crucial role [9].

2. Theoretical Approach

2.1 Hartree-Fock Energy

In our theoretical approach to calculate the Hartree-Fock energy EHF for the ^{12}C nucleus, we consider a nuclear system comprising A nucleons (N neutrons and Z protons) with spin s = ½, τ = 1/2, and mass m. The Hamiltonian of this system incorporates both the single-particle energy and a two-body interaction, represented by the equation:

$$H = \sum_{i=1}^{A} t_i + \sum_{i<j}^{A} V_{ij} \quad (1)$$

where t is the ith nucleon's kinetic energy operator and Vij is the ith and jth nucleon's two-body interaction term, including the Coulomb potential ($V = V_{NN} + V_C$). The second sum's limitation I j accounts for the fact that the interaction must be summed only once for each pair. The accurate solution to the many-body issue can be obtained if the problem is solved in the whole Hilbert space. This, however, is not possible for nuclei with A > 4. As a result, the Hilbert space is truncated to a finite model space. The price is to define an effective Hamiltonian [15–17] as follows:

$$H'_{eff} = \sum_{i=1}^{A} t_i + \sum_{i<j}^{A} (V_{eff})_{ij} \quad (2)$$

Then, instead of employing the single particle energy operator, we use the relative kinetic energy operator $(T_{rel})_{ij}$ to introduce a two-body effective Hamiltonian $H_{eff}(t_i)$.

$$H_{eff} = T_{rel} + V_{eff} \quad (3)$$

where $(T_{rel})_{ij}$ is the two-body relative kinetic energy operator between pairs of nucleons [18],

$$(T_{rel})_{ij} = \frac{(P_i - P_j)^2}{2mA} \quad (4)$$

In the no-core model space, the V_{eff} is the sum of the Brueckner G-matrix acting between two nucleons. To calculate the effective Hamiltonian, H_{eff}, we follow the same calculation procedures and strategy in Refs. [15–17]. Our current goal is to use a two-particle harmonic oscillator H-O basis with good total angular momentum J and total isospin T to generate the matrix element of the two-body part of the effective Hamiltonian ($T_{rel} + V_{eff}$) in the chosen model space. We can detach the relative coordinates from the center-of-mass coordinates when utilizing the H-O basis, which simplifies the calculations of the two-body matrix elements [18]. Here, we remind the reader of our incentives for employing the more effective of the "two infinites." The infinite short-range repulsion (V) of the core in finite-dimensional Hilbert space. The first infinite is solved by applying the Block-Horowitz theory to amputate the Hilbert space. The second infinity is eliminated by solving the Bruckner-Bethe Goldstone equation, which involves replacing the elements of the matrix V with elements of the Bruckner G-matrix in the series expansion of:

$$G(\omega) = V + V\frac{Q}{\omega - H_0}G(\omega) \quad (5)$$

where H_0 is the unperturbed single particle Hamiltonian, ω is the beginning energy, and Q is the Pauli operator that prevents particles from scattering into occupied states [10].

The system's Hartree-Fock HF energy, defined in terms of H_{eff} anti-symmetric two-body matrix elements, is:

$$E_{EH} = \frac{1}{2}\sum_{\kappa\lambda} < \lambda\mu|H_{eff}\,|\lambda\mu >_A \quad (6)$$

where |λμ> are the single particle HF states. We can expand the HF state in terms of H-O states as:

$$|\lambda > = \sum_{\kappa} C_{\kappa}^{\lambda}\,|k > \quad (7)$$

where k denotes the collection of quantum numbers, $k \equiv (\bar{k}, m_\lambda, m_{\tau\lambda})$ and $\bar{k} \equiv (n_k, l_k, j_k)$. The coefficients satisfy the condition $\sum_{\kappa}\left|C_{\kappa}^{\lambda}\right|^2 = 1$. Thus, the HF energy in terms of H-O basis is written as:

$$E_{HF} = \frac{1}{2}\sum_{\lambda\mu}\sum_{\kappa\kappa'}\sum_{\kappa_1\kappa_2} C_{\kappa}^{\lambda *}C_{\kappa'}^{\lambda}\; C_{\kappa_1}^{\mu *}C_{\kappa_2}^{\mu}\left\langle\kappa\kappa_2\left|H_{eff}\right|\kappa'\kappa_2\right\rangle_A \quad (8)$$

The coefficients C_{κ}^{λ} is calculated using the variational principle,

$$\frac{\partial}{\partial C^*}\left(E_{HF} - \sum_{\lambda}\left(\sum_{\kappa} C_{\kappa}^{\lambda *}C_{K}^{\lambda} - 1\right)\epsilon_{\kappa}\right) = 0 \quad (9)$$

where C is one of the C_K^{λ}. The constants ϵ_κ are the Lagrange multipliers, which principle expresses the single-particle energies. We get this by plugging Eq. (9) into Eq. (8):

$$\sum_{\kappa'} C_{\kappa'}^{\lambda}\left(\sum_{\kappa_1\kappa_2\mu} C_{\kappa_1}^{\mu *}C_{\kappa_2}^{\mu}\left\langle\kappa\kappa_1\left|H_{eff}\right|\kappa'\kappa_2\right\rangle_A\right) = C_{\lambda}^{\kappa}\,\epsilon_{\lambda} \quad (10)$$

We define,

$$h|\lambda \geq \epsilon_{\lambda}|\lambda >$$

$$\langle k|h|\lambda\rangle = \epsilon_{\lambda}\langle k|\lambda\rangle$$

$$\sum_{\kappa'}\langle k|h|k'\rangle = C_{\kappa}^{\lambda}\epsilon_{\lambda} \quad (11)$$

By equating Eqs. (10) and (11), we get:

$$\langle k|h|k'\rangle = \sum_{\kappa_1\kappa_2\mu} C_{\kappa_1}^{\mu *}C_{\kappa_2}^{\mu}\left\langle\kappa\kappa_1\left|H_{eff}\right|\kappa'\kappa_2\right\rangle_A \quad (12)$$

Equation (11) is solved by selecting an acceptable set {|k>} so that the series for |λ> converges quickly, allowing us to truncate it after a few terms. Once {|k>} is picked, iteration can be used to try to locate a solution. To do so, one estimates a set of values C_{κ}^{λ} from which $\langle k|h|k'\rangle$ is calculated. After that, Eq. (12) is solved for a new set $\{C_{\kappa}^{\lambda}\}$ and $\langle k|h|k'\rangle$ is calculated. This procedure is repeated until a self-contained solution is found.

The single-particle density matrix is defined as follows:

$$\sum_{\mu} C_{\kappa_1}^{\mu}C_{\kappa_2}^{\mu} = \rho\kappa_1\kappa_2 \quad (13)$$

By incorporating the constraint term β⟨N|r^2|N'⟩ in Eqs. (9) and (12), the radial constraint is introduced to the issue, where β is the constraint parameter. The radial constraint acts as a static external force on the nucleus, compressing or expanding it. If β is negative (positive), the nuclear radius decreases (increases) from its equilibrium value of β = 0. We employ a spherical Hartree-Fock (SHF) computer code based designed according to Eqs. (11) and (12).

2.2 Root-Mean-Square Radius (R_{rms})

The root-mean-square r_{rms} radius is an essential indicator for the change of the nuclear density distribution due to the compression of the nucleus. We calculate the r_{rms} using the following equation [19]:

$$r_{rms} = (\langle r^2\rangle)^{1/2} = \left(\frac{\int r^2\rho(r)d^3r}{\int \rho(r)d^3r}\right)^{1/2} \quad (14)$$

where ρ is the single-particle density matrix. The wave function is written in the H-O coordinate, starting from an anti-symmetrized Slater determinant, which contains the component of the center-of-mass motion. Consequently, the single-particle density is calculated with the wave function includeing contribution from the center-of-mass motion [19].

3. Methodology and Scaling

We use the H-O basis with a value of $\hbar\omega$ = 14MeV to evaluate the H_{eff} matrix elements. We use the scaling rule of Refs. [15–17] to make applying H_{eff} to a wide range of nuclei as simple as feasible. That is, if we refer to a matrix element of an operator H_{eff} as ⟨H_{eff}⟩, we are assuming that it was calculated on an oscillator basis with ħω'. The matrix elements of H_{eff} on a basis with ħω' are roughly provided by:

$$\langle H_{eff}\rangle' = \frac{\hbar\omega'}{\hbar\omega}\langle H_{eff}\rangle \quad (15)$$

As a result, when we employ the scale element of H_{eff} in 6-space for ^{12}C, we acquaint

the factor $\hbar\omega'$. In addition, the overall factors λ_1 and λ_2 are introduced to adjust the kinetic energy and effective nucleon-nucleon interaction matrix elements, respectively. To explore the sensitivity of E_{HF} and r_{rms} to changing the adjusting parameters, we have investigated how E_{HF} and r_{rms} responded to different values of λ_1, λ_2, and $\hbar\omega$ without compression until an agreement between E_{HF} and r_{rms} with the corresponding experimental quantities is reached.

Table 1 shows the fitted values of $\hbar\omega'$, λ_1, and λ_2 for ^{12}C at equilibrium. The numerical value of λ_1 is less than unity because the kinetic energy operator (T_{rel}) is a positive definite operator, and if it is normalized into a finite model space by itself, its magnitude will be reduced. However, the numerical value of λ2 is more than unity to compensate for the absence of acceptable linking when the full Hilbert space is truncated to a finite space model. We utilize a big model space with six primary shells, or 21 nucleon orbitals, each with definite quantum numbers, *n, l, s, and J*, in our calculations.

TABLE 1. Adjustment values for the ^{12}C nucleus in 6- shells using Nijmegen and RSC potentials to achieve agreement between HF and experimental data [20].

Potential $\hbar\omega'$ (MeV) λ_1	λ_1
Nijmegen 8.454 0.976	1.200
RSC 10.104 0.973	1.420

The major steps of one iteration of the constraint SHF computations are now outlined. The number of nucleons, the number of HF occupied states, the 2J, l, n values of the H-O orbitals, the H-O constants ħω, ħω', and the number of repetitions are read and saved. According to the formulations in Eqs. (11) and (12), the initial quantities to be calculated and stored are the HF Hamiltonian matrix elements. To do so, we begin by reading and storing nucleon densities of unity. The matrix elements of the effect Hamiltonian $\left(i.e.T_{rel},\left(V_{eff}^{NN}=G\right),V_{coulomb}\right)$ are retrieved and scaled with λ_1, λ_2, $\hbar\omega'$. A second set of HF Hamiltonian matrix elements, $\langle N|h|N'\rangle'$, is calculated using this set of HF Hamiltonian matrix elements. It includes the term constraint and is defined as follows:

$$\langle N|h|N'\rangle' = \langle N|h|N'\rangle - \beta\langle N|r^2|N'\rangle \qquad (16)$$

The associated eigenvalues and eigenvectors are calculated using the second set of HF Hamiltonian matrix elements. New nucleon densities are calculated using the eigenvectors. Eq. (14) is used to calculate the rms radius using the new nucleon densities. Finally, using the HF Hamiltonian matrix elements from the first set and new nucleon densities, the Hartree-Fock Energy (EHF) is determined using Eqs. (11) and (12), bringing the first iteration to a close. The second iteration starts with the nucleon densities computed in the first repetition and calculates the delineated quantities in the same way as the first repetition. Until a confluent solution is found, the accordant process continues.

4. Results and Discussion:

We find the equilibrium (r_{rms}) and E_{HF} for ^{12}C using RSC (Nijmegen) potentials, r_{rms} = 2.3508*fm* (r_{rms} = 2.3498*fm*) (*fm* = 10^{-15}m), and E_{HF} = −92.174MeV (E_{HF} = −92.167 MeV), respectively. The experimental nuclear radius for ^{12}C is r_{exp} = 2.35*fm*, while the experimental binding energy is E_{bind} = −92.162MeV according to Ref. [20]. There is also an agreement between our results and the Navratil results [9], where the radius energy and the binding energy in the Navratil results, respectively, are 2.228 *fm*, 92.353MeV in the CD Bonn case and 2.228fm, 92.195 in Argonne V8 case. In addition, we discover that the occupied orbitals are $0s_{1/2}$ and $0p_{3/2}$, which is consistent with the standard shell model.

In six-oscillator shells, the Hartree-Fock energy E_{HF} is plotted as a function of the root-mean-square radius (r_{rms}) of ^{12}C as shown in Fig.1. In prior studies [15], we found that compressing the nucleus (i.e. reducing its volume) lowers the binding energy of the nucleus. In the case of ^{12}C, lowering its volume to about 12% of its equilibrium volume reduces the binding energy by 2% utilizing RSC potential. Furthermore, when we reduce the nuclear volume by around 6%, the change in nuclear binding energy is just about 1%. However, by employing the Nijmegen potential for the same decrease in nuclear volume as the volume at equilibrium, the binding energy will be reduced by 11% and 1%, respectively. As a result, as the nucleus is compressed, the nuclear equation of state stiffens. We also see that the RSC potential softens the equation of state more than the Nijmegen potential. Furthermore, the curve for Nijmegen potential reaches zero binding energy quicker than RSC potential, and

the nuclear binding energy for Nijmegen potential is greater than the binding energy for RSC potential at substantial static compression. The ground state features of the ^{4}He nucleus under large static compression were explored in Refs. [21, 22] using Nijmegen and RSC potentials, and they came to the same conclusion, which was one of our motives for employing the same two distinct potentials for the ^{12}C.

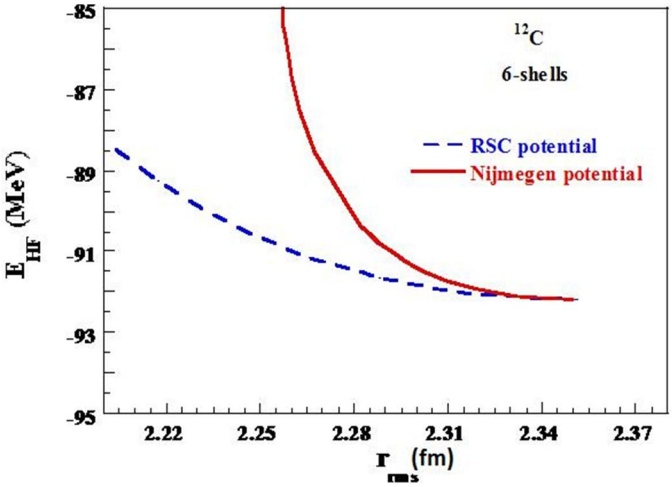

FIG. 1. Energy EHF of Constrained Spherical Hartree-Fock Vs. of r_{rms} for ^{12}C in 6-oscillator/shells. Potentials from RSC and Nijmegen.

Fig. 2 shows the single-particle energy levels (SPE) as a function of the r_{rms} in six oscillator shells. It is important to understand that the orbital ordering agrees with the standard shell model's orbital ordering. Furthermore, in both potentials, we detect the splitting of the levels in each shell as a measure of the intensity of L-S coupling. This is also clear from the shifting down of $0f_{7/5}$ orbit from p-f shell to s-d shell. However, as the nucleus' compression is increased, L-S coupling gets weaker. Furthermore, as the nucleus' compression is increased, the orbits curve higher. When utilizing the Nijmegen potential, the Single Particle Energy (SPE) Levels are bending upwards faster. This is detailed in the results of ^{4}He [15], and it is owing to the effect of the nucleon's kinetic energy, which becomes more significant than the nucleon's attractive mean field. Furthermore, the SPEs utilizing the Nijmegen potential are less bound than the SPEs using the RSC potential, especially as the nucleus is compressed more and more. Moreover, the underlying microscopic Hamiltonian entirely forms the energy spectrum. In the dominating nucleon orbitals, this produced energy spectrum corresponds to the theoretical shell model's expected ordering. Furthermore, the energy levels have distinct gaps between the shells. One of the most striking findings is that in the compressed nucleus, the orbitals nearest to binding energy are more delicate for the two potentials.

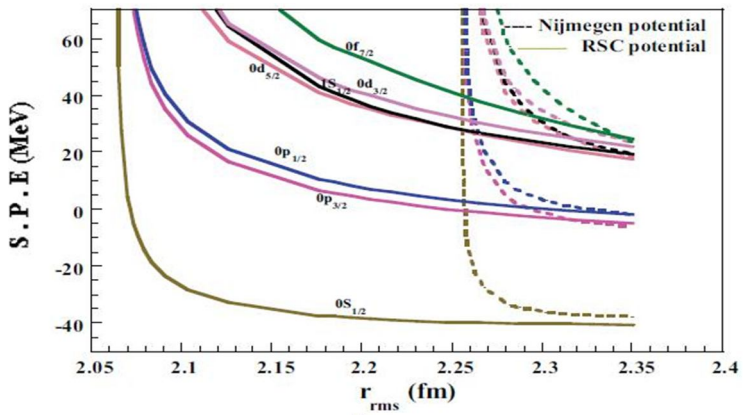

FIG. 2. Single particle energy (S.P.E.) vs. rrms for ^{12}C in 6-oscillator shells. Potentials from Nijmegen and (RSC).

Fig. 3 illustrates the radial density distribution for neutrons ρ_n,, protons ρ_p, and $\rho_{total} = \rho_n + \rho_p$ using the Nijmegen potential at equilibrium (i.e. at r_{rms} = 2.35fm). Figure 4 illustrates the radial density distribution at equilibrium (r_{rms} = 2.35*fm*) and at a significant static compression (r_{rms} = 2.26*fm*) using Nijmegen potential. In Fig. 5, we compare ρ_{total} at two different values of r_{rms}; at r_{rms} = 2.35*fm* (i.e. equilibrium) and at r_{rms} = 2.06*fm* using RSC potential. In Fig. 6, we compare ρ_{total} at two different potentials (Nijmegen and RSC) at equilibrium (r_{rms} = 2.35*fm*). Furthermore, in Fig. 7, we compare the total at two different potentials (Nijmegen and RSC) at large static compression (r_{rms} = 2.26*fm*). The radial density distribution function for neutrons ρ_n, protons ρ_p, and sum ρ_{total} of the nucleus as a function of radial distance from the nucleus center at equilibrium (i.e. rrms = 2.35 fm) using the Nijmegen potential is shown in Fig. 3.

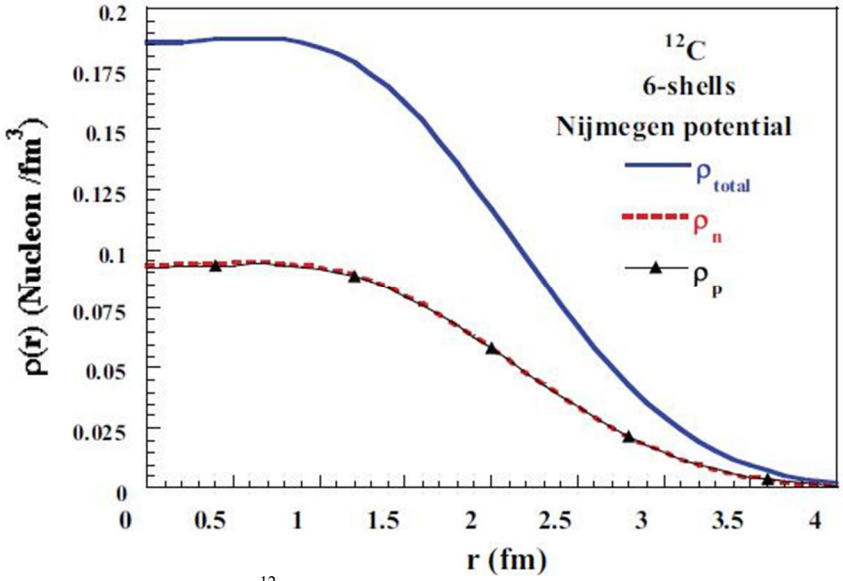

FIG. 3. Radial density distribution for ^{12}C as a function of nuclear radius r(*fm*) at equilibrium (r_{rms} = 2.35*fm*) using Nijmegen potential.

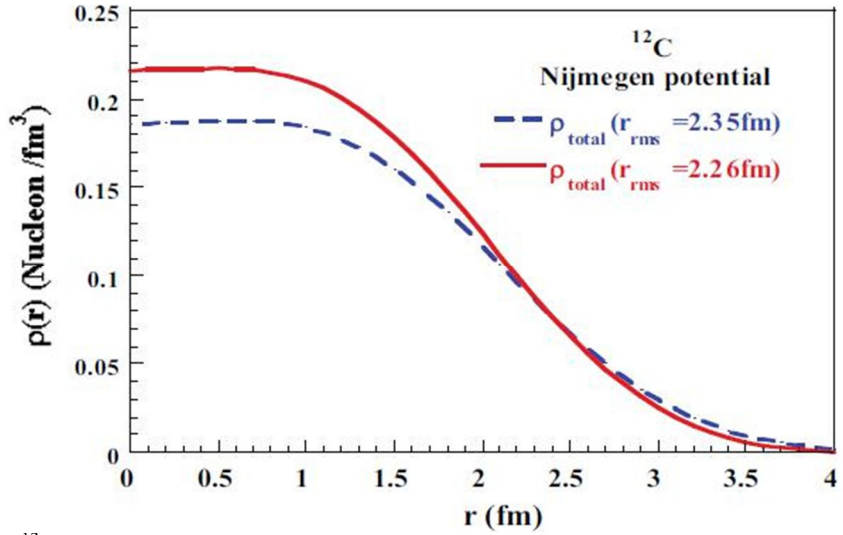

FIG. 4. ρ_{total} for ^{12}C at equilibrium (r_{rms} = 2·35*fm*) and large static compression (r_{rms} = 2.26*fm*) vs. of nuclear radius r(*fm)* utilizing Nijmegen potential.

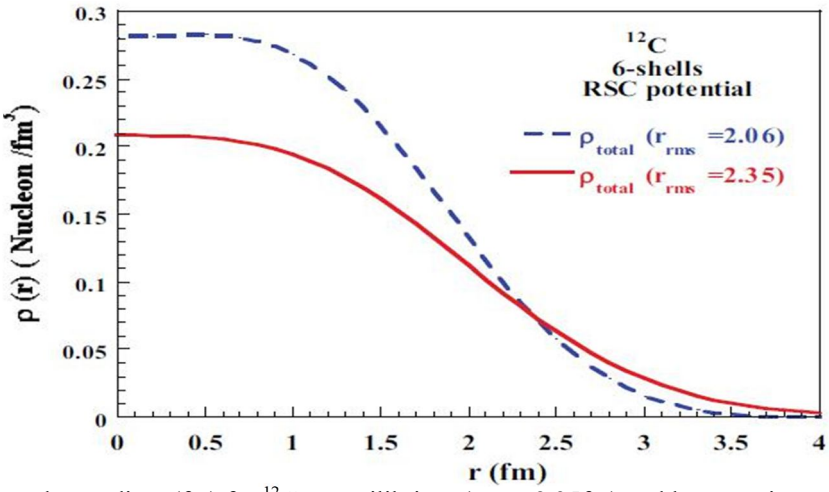

FIG. 5. ρ_{total} vs. nuclear radius r(fm) for ^{12}C at equilibrium (r_{rms} = 2.35fm) and large static compression (r_{rms} = 2.06fm) utilizing RSC potential.

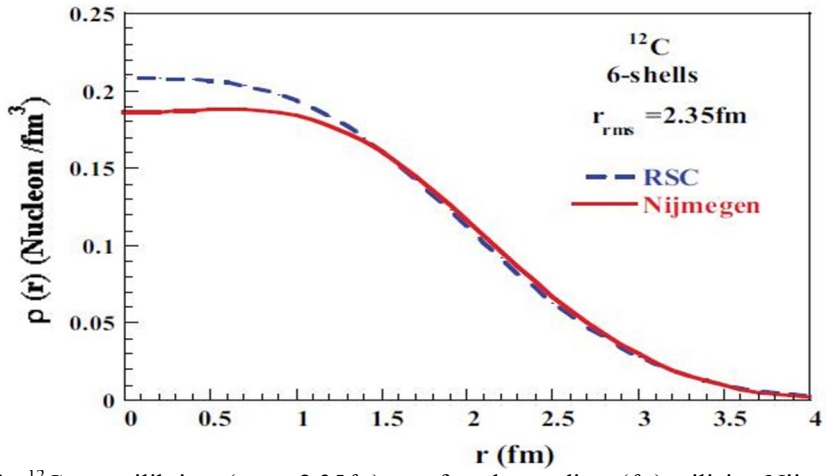

FIG. 6. ρ_{total} for ^{12}C at equilibrium (r_{rms} = 2.35*fm*) vs. of nuclear radius r(*fm*) utilizing Nijmegen and RSC potentials.

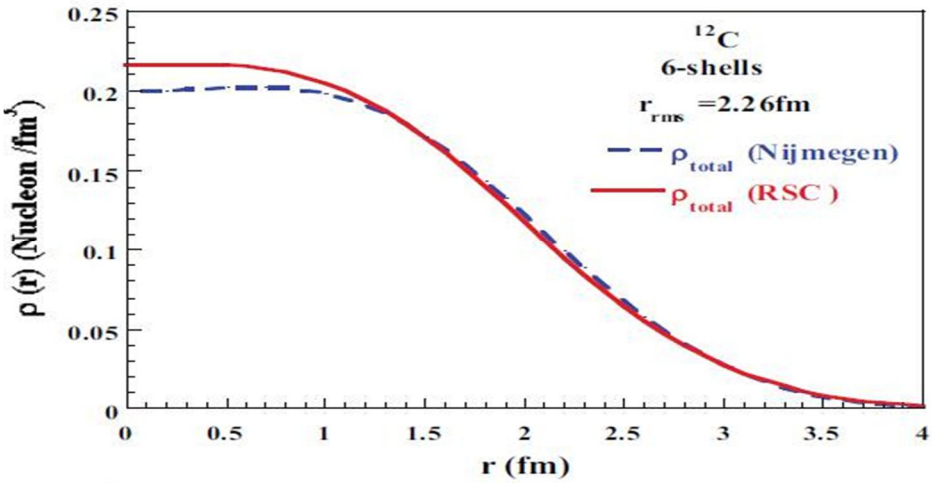

FIG. 7. ρ_{total} for ^{12}C at large static compression (r_{rms} = 2.26*fm*) utilizing Nijmegen and RSC potentials.

The neutrons' and protons' densities are almost the same except in the interior region, where the neutrons are denser than protons. The Coulomb repulsion force between the protons causes this variation in density. Thus motivated, we seek to test the extent of the compression of the nucleus and the sensitivity of the equation of the state to the potential under the compression. The total radial density distribution ρ_{total} has been shown based on the radial distance from the center of the nucleus at equilibrium (i.e. r_{rms} = 2.35fm) and at (r_{rms} = 2.26fm). On the one hand,

using the Nijmegen potential (Fig. 4) and RSC at equilibrium (i.e. r_{rms} = 2.35fm) and at (r_{rms} = 2.06fm), we discovered that if the nucleus volume is lowered by 11% of the situation of equilibrium, the radial density increases by around 2.10 of its value in the case of equilibrium. On the other hand, utilizing RSC, if the volume is lowered by 67% of the equilibrium situation, the radial density increases by around 2.3 of its value as shown in Fig. 5. As seen in Fig. 4, as the nucleus is compressed, the nuclear density gets denser on the inside and less dense in the exterior (i.e. closer to the nucleus' surface). As a result, the surface of the nucleus becomes more sensitive as the load is increased. However, in Fig. 5, we notice the same features as in Fig. 4, that is the interior of the nucleus becomes denser than the exterior as we compress the nucleus. There is one difference, though: increasing the nuclear density is more obvious using RSC than using Nijmegen potential. Figure 6 shows the total radial density distribution ρ_{tota} with the two potentials at large static compression (r_{rms} = 2.26 fm) (Nijmegen and RSC). The following are our conclusions. First, the nuclear density became denser on the inside and smaller dense in the exterior (i.e. close to the surface of the nucleus) as the nucleus compressed for the two potentials. This means as the static load is increased more and more, the surface of the nucleus becomes more and more responsive. Second, using RSC potential, the rise in nuclear density with compression in the interior is more prominent than using Nijmegen potential. The nuclear density using Nijmegen potential is closer to the nuclear saturation density calculated using the empirical formulas, ranging from 0.15 to 0.177 fm^{-3}. Finally, Fig. 7 shows the overall radial density distribution with the two potentials at equilibrium (r_{rms} = 2.35fm) (Nijmegen and RSC). The interior region of the nuclear density is bigger when employing RSC than when utilizing Nijmegen potential, as shown in this figure. In the exterior region, the situation is reversed.

5. Conclusions

By using RSC and Nijmegen potentials, we established that for ^{12}C, the values of equilibrium root-mean-square radius (r_{rms}) are 2.351*fm* and 2.35*fm*, while the corresponding EHF energies are -92.174MeV and -92.167MeV, respectively. Experimental data indicates that the nuclear radius for ^{12}C equals 2.35*fm* and the value of the binding energy equals -92.162MeV [20]. The minimum rrms radii for ^{12}C obtained are 2.063*fm*, and 2.255*fm*, while the corresponding EHF are -49.579MeV and -82.444MeV, for RSC and Nijmegen potentials, respectively.

When it comes to ^{12}C, RSC can compress the nucleus to a smaller size than Nijmegen potential. With the exception of the inner region, where neutrons are denser than protons, the densities of neutrons and protons are about equal at equilibrium. The Coulomb repulsion force between protons is responsible for the difference in densities. When the two potentials (Nijmegen and RSC) are in equilibrium, the RSC potential has a higher nuclear density than the Nijmegen potential. In the exterior region, the scenario is reversed. Furthermore, the orbit ordering is equal to the standard shell model's orbit ordering. The space between the shells is clearly visible. The separation of the levels in each shell indicates that L-S coupling is sufficient in strength when either of the potentials is applied. This is also clear from shifting down the $0f_{7/5}$ orbit from the p-f shell to the s-d shell. As the static strain on the nucleus increases, the L-S coupling gets stronger. In addition, the levels curve up as we compress the nucleus further, and this curvature is more rapid when using Nijmegen potential. This signifies that the nucleus' kinetic energy, which is a positive quantity, is becoming increasingly significant over the nucleon's attractive mean field. Finally, we note that while utilizing Nijmegen potential, the SPEs are greater than when using RSC potential, especially at high compression.

Acknowledgments

We gratefully acknowledge support from the Hashemite University.

Conflict of interest

The authors have no conflicts to disclose.

References

[1] Stevenson, P.D., Rikovska Stone, J. and Strayer, M.R., Phys. Lett. B, 545 (2002) 291.

[2] Preston, M. and Bhaduri, R., "Structure of the Nucleus", 1st Ed., (New York and Tornto, Pergamon Press, 1975) p 10-65.

[3] Stoks, V., Klomp, T. and de Swart, Phys. Rev. C, 49 (6) (1994) 2950.

[4] Lassey, K. and McKellar, B., Phys. Rev. C, 11 (1975); Erratum Phys. Rev. C, 12 (1975) 721.

[5] Machleidt, R., Phys. Rev. C, 63 (2001) 1.

[6] Wiringa, R., Stoks, V. and Schiavilla, R., Phys. Rev. C, 51 (1) (1995) 39.

[7] Bogner, S., Kuo, T.T.S., Coraggio, L., Covello, A., Itaco, N. and Kuo, T., Phys. Rev. C, 65 (051301(r)) (2002) 1.

[8] Navratil, P. and Barrett, B., Phys. Rev. C., 54 (6) (1996) 2986.

[9] Navratil, P., Vary, J. and Barrett, B., Phys. Rev. Lett., 84 (2000) 5728.

[10] Zheng, D., Barrett, B., Jaqua, L., Vary, J. and McCarthy, R., Phys. Rev. C., 48 (3) (1993) 1083.

[11] Barrett, B., Mihaila, B., Pieper, S. and Wiringa, R., Nucl. Phys, News, 13 (1) (2003) 17.

[12] Ring, P. and Schuck, P., "The Nuclear Many Body Problems", (Springer, Berlin, 1980) p. 37-42.

[13] Hasan, M. and Vary, J., Phys. Rev. C, 50 (1) (1994) 202.

[14] Hasan, M., Lee, T. and Vary, J., Phys. Rev. C, 56 (6) (1997) 3063.

[15] Abu-Seileek, M., J. Appl. Math. Phys., 6 (2018) 458.

[16] Deville, G., Valdes, A., Andrei, E.Y. and Williams, F.I.B., Phys. Rev. Lett., 53 (6) (1984) 588.

[17] Anderson, B.D., Chittrakarn, T., Baldwin, A.R., Lebo, C., Madey, R., Tandy, P.C., Watson, J.W., Brown, B.A. and Foster, C.C., Phys. Rev. C, 31 (4) (1985) 1161.

[18] Hasan, M., Ph.D. Dissertation, The University of Arizona, (1987).

[19] Hu, B., Xu, F., Sun, Z., Vary, J. and Li, T., Phys. Rev. C, 94 (014303) (2016) 1.

[20] Ajzenberg, F.S., Nucl. Phys. A, 475 (1987) 1.

[21] Tilley, D.R., Waller, H.R. and Hasan, H.H., Nucl. Phys. A, 474 (1987) 1.

[22] Abu-Seileek, M., Iran. J. Sci. Technol., 43 (2019) 1365.